

# Computational method to estimate Single Event Upset rates in an accelerator environment

M. Huhtinen, F. Faccio

*CERN, CH-1211 Geneva 23, Switzerland*

---

## Abstract

We present a new method to estimate Single Event Upsets (SEU) in a hadron accelerator environment, which is characterized by a complicated radiation spectrum. Our method is based on first principles, i.e. an explicit generation and transport of nuclear fragments and detailed accounting for energy loss by ionization. However, instead of simulating also the behaviour of the circuit, we use a Weibull fit to experimental heavy-ion SEU data in order to quantify the SEU sensitivity of the circuit. Thus, in principle, we do not need to know details about the circuit and our method is almost free of adjustable parameters – we only need a reasonable guess for the Sensitive Volume (SV) size. We show by a comparison with experimental data that our method predicts the SEU cross sections for protons rather accurately. We then indicate with an example how our method could be applied to predict SEU rates at the forthcoming LHC experiments.

*Key words:* SEU, single event upset, radiation tolerance

---

## 1 Introduction

Single Event Upsets (SEU) have always been a serious concern for space electronics [1], but so far the high-energy physics community has paid little attention to this type of radiation effect. With the forthcoming commissioning of the Large Hadron Collider (LHC) at CERN the radiation levels at large experiments are significantly increased with respect to past experience. In the very hostile environment created by the LHC, SEU could become an important issue. It will certainly not be a problem if a small fraction of the enormous data stream from a hadron collider experiment is corrupted by SEUs. The potential danger, however, is loss of some vital detector control functions due to memory upsets.

It is a well established fact that a SEU is caused by a very high energy deposition in a small volume of the electronics chip. The charge released along the ionizing particle path, or at least a fraction of it, is collected at one of the microcircuit nodes, and the resulting current transient might generate a SEU. The most sensitive regions of a microelectronic device are the reverse-biased p/n junctions, where the high electric field is very effective in collecting the charge by drift. Charge is also collected by diffusion, and some of it recombines before being collected.

The effect of the collected charge depends on the circuit and, inside the same circuit, on the node where the collection occurs. The plasma effect, i.e. self-screening of the charge might also reduce the charge collection efficiency for very dense ionization.

DRAMs have historically been sensitive to SEU as they rely on passive charge storage to represent information. Their logic state can therefore be easily corrupted by the charge collection following a strike by a highly ionizing particle. In SRAMs, the situation is different because of the presence of an active feedback typical of the cross-coupled inverter pair. In the SRAMs, there is always one "on" transistor driving the collected charge to either Vdd or Vss, and this mechanism is in competition with the propagation of the error along the feedback represented by the other inverter gate. In both the DRAM and the SRAM cases, whether or not the circuit upsets is determined by a combination of both the charge collection dynamics (collection efficiency, time constants, ...) and the circuit response to the consequent current transient. Moreover, these two characteristics are strictly related, as fast collection of a first portion of the charge might influence the collection efficiency for later arriving fractions of the charge.

In a somewhat simplified picture, i.e. neglecting charge collection efficiencies, time constants and other related effects, we can assume that the SEU occurrence depends on two parameters of the device:

- (1) The Sensitive Volume (SV) within which the ionization has to take place for the charge to be collected on the node.
- (2) The Critical Energy ( $E_{\text{crit}}$ ) which has to be exceeded by the deposited ionizing energy ( $E_{\text{dep}}$ ) within the SV in order to trigger an upset.

In a most simplistic model the SV can be assumed to have sharp boundaries and  $E_{\text{crit}}$  to be step-like. In a slightly improved model we can use experimental heavy-ion data which implicitly include some information about charge collection in the SV and give a smooth transition from zero upsets to the saturated condition.

## 2 Origin of high ionization

The energy loss,  $dE/dx$  or LET (linear energy transfer), of a minimum ionizing particle (e.g. a proton of about 2 GeV) is 3.9 MeV/cm in silicon. This energy loss increases rapidly with decreasing energy of the particle. Most particle physicists are used to think in terms of the Bethe-Bloch formula which indicates an unlimited increase. In reality the Bethe-Bloch equation loses validity at sufficiently low energies and the  $dE/dx$  curve reaches a maximum before it turns into a decrease. For a proton this maximum is at about 100 keV of kinetic energy.

A heavy ion is characterized by a charge ( $Z$ ) greater than unity and at very high energies the  $dE/dx$  scales roughly as  $Z^2$ . At low energies the ion is not fully ionized and the difference to a proton is reduced. Another important aspect is that with increasing ion mass the non-ionizing energy loss increases. While non-ionizing effects are almost negligible for protons they have to be taken into account when studying the stopping of heavy ions. Theoretical energy loss curves in silicon are shown in Fig. 1 for some typical ion species.

At LHC the heavy ions will be produced by hadronic interactions, mainly induced by protons,

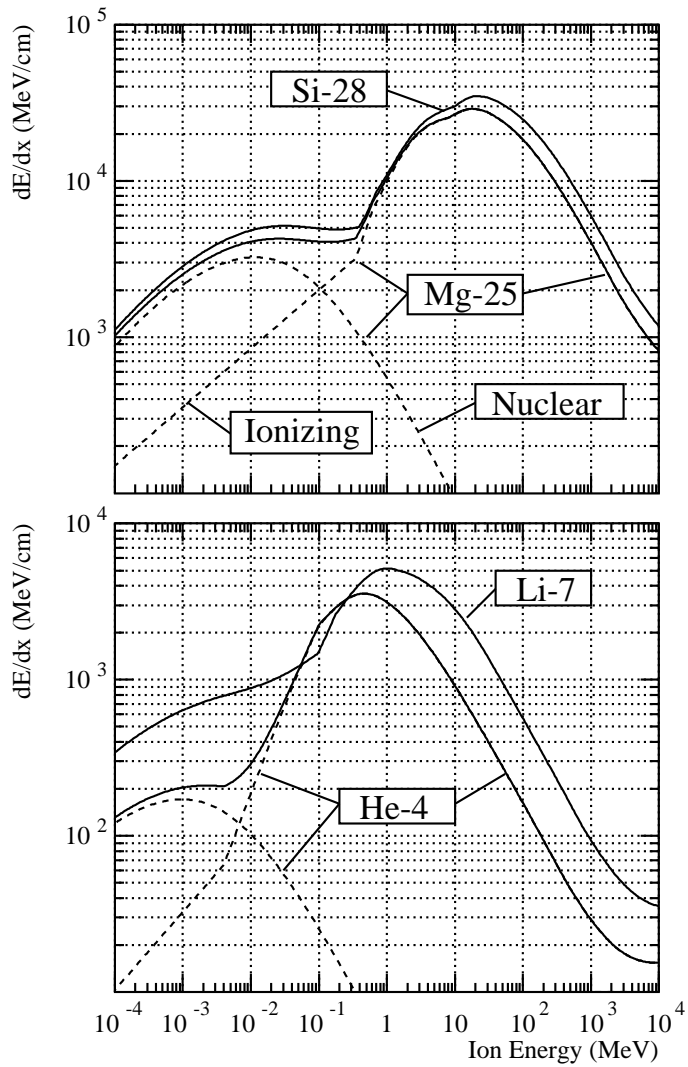


Fig. 1. Energy loss of some ion species in silicon ( $\rho=2.33 \text{ g/cm}^3$ ) as a function of the kinetic energy of the ion.

pions and neutrons. Such interactions typically will produce a shower of secondary particles and one nuclear recoil – in some cases there can be several fragments.

The recoils typically have rather low energies, rarely exceeding 10 MeV. Thus their range is very limited (below about  $10 \mu\text{m}$ ) which means that they have to be produced locally in the electronics chip itself in order to induce a SEU. From Fig. 1 we can already get a first feeling what order of magnitude the energy loss could be. We can see, for instance, that a 10 MeV silicon recoil would have a  $dE/dx$  of about  $30 \text{ GeV/cm}$  – about 4 orders of magnitude above minimum ionizing. For an  $\alpha$ -particle the maximum is reached around 500 keV of kinetic energy and its value is roughly one order of magnitude lower than for silicon.

While a lot of effort has been devoted to a study of secondary particle emission from inelastic nuclear reactions, very few experiments have paid attention to the characteristics of the slow recoil ion. Also – and one should say consequently – not much emphasis has been put into ensuring that the recoil nucleus is properly produced by standard particle physics simulation codes. Fortunately the models included in modern codes start to be reasonably realistic and should automatically produce a fairly correct recoil ion distribution. Most of our interest is in the energy region below a few GeV, where a lot of effort has been devoted to pre-equilibrium intranuclear cascade models. Such a code [2] is included in the FLUKA simulation package [3] and provides the source for our simulations whenever the incident particle has an energy above the reaction threshold (or 20 MeV in case of neutrons). Energies exceeding the upper limit of the pre-equilibrium model are rather rare in the LHC minimum bias spectrum. Thus, even though recoils produced by multi-GeV hadronic interactions are likely to be less reliably described, their relative importance should remain small.

Low-energy neutrons form another important particle category at LHC. For neutrons we define low-energy as  $<20$  MeV, up to which comprehensive neutron cross section data is available. In this domain reactions are generated directly from the information contained in the ENDFB-VI cross section tabulations without any involvement of the FLUKA code.

A third class of reactions requiring attention is elastic scattering. Most of this is directed to very forward angles and does not produce recoils which would have enough energy to trigger a SEU. In some rare cases, however, when the scattering angle is large, the silicon nucleus can receive a non-negligible recoil energy. For low energy neutrons the elastic angular distributions are given in the cross section files and are thus automatically included. At energies above 20 MeV we use a relatively simple optical model based on Glauber theory [4] to calculate the elastic differential cross section. Although the Glauber model is not really valid at low energies, which become comparable to the binding energy of nucleons, it still produces a reasonably good agreement with experimental scattering data. However, for protons below 95 MeV we use fits to experimental data instead of the Glauber model. This description of elastic scattering is of sufficient accuracy for us, in particular, because our results will indicate that the elastic scattering at energies above 20 MeV does not give an important contribution to the SEU rate. This is true even though our model tends to overestimate scattering to large angles – i.e. gives an excess of energetic recoils.

## 2.2 Energy loss of slow fragments

A central part of our simulation work concerns the stopping of the produced nuclear fragments. The theory describing the energy loss of slow ions in solids is provided in [5]. We have followed the lines of the TRIM code given in [5] but with some modifications which make the code more suitable for our application and allow to treat a full atomic cascade. For the latter purpose we have introduced the explicit production of secondary recoils when the ion collides with lattice atoms.

Fig. 2 shows the ranges of some ion species as a function of the energy. We can see that for the

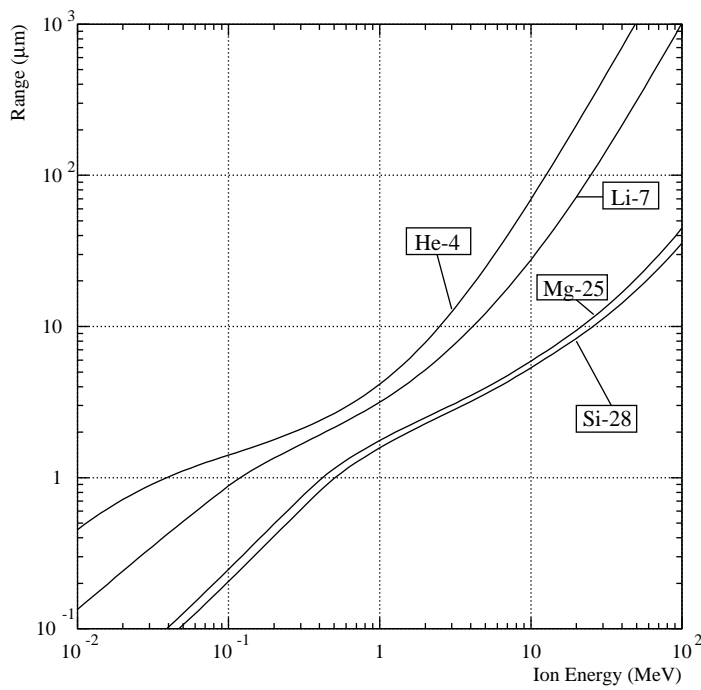


Fig. 2. Ranges of a few ion types in silicon ( $\rho=2.33 \text{ g/cm}^3$ )

energies and ion types of interest for us the ranges are typically a few microns. Although an  $\alpha$ -particle with 10 MeV kinetic energy can traverse several tens of microns in silicon the short ranges – and much higher  $dE/dx$  – of heavy fragments suggest that we have to put our main emphasis on events in close vicinity of the SV.

Not only the range of a fragment is interesting, but also the maximum ionization it can deposit along a given path-length. Due to the very large energy loss  $dE/dx$  varies rapidly and the curves in Fig. 1 have to be integrated in small steps. The results of such an integration is shown in Fig. 3 for pre-determined path lengths of 1, 2 and 4  $\mu\text{m}$ . All curves reach a definite saturation value which means that the range is large enough so that the integral over the given path length is centered around the maximum energy loss. Another interpretation of the curves is that up to the saturation point the maximum loss is always in the first track segment of the given length. For energies beyond the saturation point the maximum appears somewhere further down the track. A very interesting feature is that the ionization of an  $\alpha$ -particle is actually higher than that of silicon at low energies. The reason is that the silicon ion loses a significant portion of its energy by non-ionizing processes whereas most of the energy loss of the  $\alpha$  goes into ionization.

It should be remarked that both Fig. 2 and Fig. 3 are based on a simple integration of the energy loss, i.e. direction changes of the ion are not considered. Thus the range gives an upper limit for the penetration depth of an ion. Correspondingly the maximum ionization at low ion energies might be slightly underestimated because the ion is likely to undergo several random scatterings just before stopping. In our full SEU simulations all these scattering effects are properly accounted for.

The energy loss of high energy hadrons in thin layers shows the typical Landau distribution,

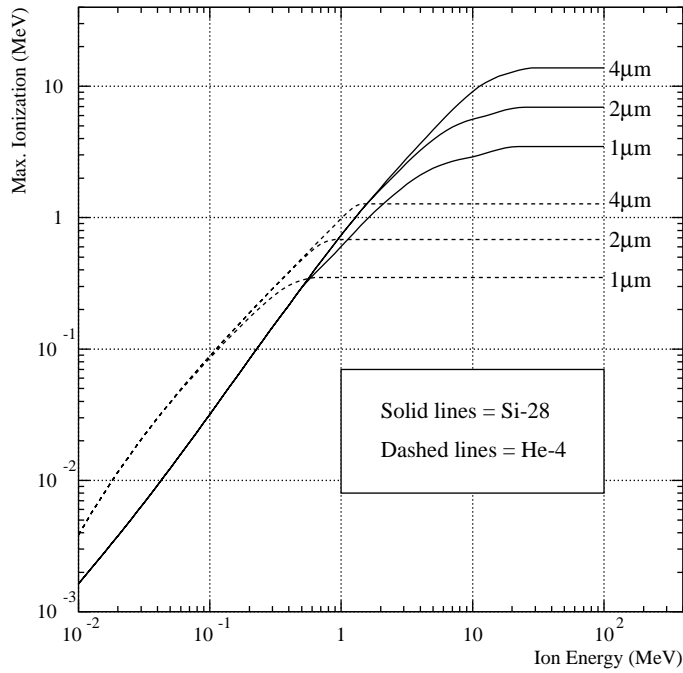


Fig. 3. Maximum ionization loss of a few ion types in silicon ( $\rho=2.33 \text{ g/cm}^3$ ). The curves show the maximum of the integral of ionizing  $dE/dx$  over the indicated path length.

where the tail corresponds to energetic knock-on electrons. The energy transfer is limited by kinematics and has a strong velocity dependence. Compared with the large ionization such hard knock-on electrons are negligible for slow heavy ions. However, the ion can also scatter on atoms of the target material and in these cases the energy transfer can be substantial. Such scattering is taken into account in our simulation and if the energy transfer is large enough the target atom is explicitly transported.

### 3 Simulation geometry and methods

The most important ingredient for setting up the simulation geometry is to decide the shape and volume of the SV. These will depend on the device to be studied and thus no single choice can be made. In order to get some feeling how important these parameters are for our results we make some of our studies with different SV sizes, namely:  $1 \times 1 \times 0.5 \mu\text{m}^3$ ,  $1 \times 1 \times 1 \mu\text{m}^3$ ,  $1 \times 1 \times 2 \mu\text{m}^3$  and  $2 \times 2 \times 2 \mu\text{m}^3$ , where the last value always gives the thickness of the sensitive layer.

Due to the small size of the SV it is quite challenging to reach sufficient statistics in the transport simulations. To increase the number of fragments traversing the SV we use a few relatively modest biasing methods. Due to the short range of fragments it is sufficient to consider only a region relatively close to the SV. But some  $\alpha$ s can have ranges of up to  $100 \mu\text{m}$ . It is unlikely that these will have a big influence, but they should not be completely omitted. Thus we preferably generate the event close to the SV and compensate this bias by assigning statistical weights to

the fragments depending at what depth they are produced in the silicon. Nevertheless, using only one SV in a big volume would still lead to a waste of many events. This is reduced by using a lattice of SV:s spaced sufficiently so that correlations, i.e. same fragment hitting two SV:s, become negligible. On 'top' of the SV we always have a  $6\ \mu\text{m}$  thick layer of silicon to simulate the passivation layers of the IC, mainly composed of silicon dioxide (equivalent to silicon for our aims). In other directions we have  $50\ \mu\text{m}$ . In low energy neutron interactions the  $(n,\alpha)$  events are likely to be the most significant to generate SEU. In order to increase statistics on these relatively rare events we sample each event channel with equal probability and assign statistical weights according to the true partial cross section.

When we simulate proton test results we always assume that the proton enters at an angle of 90 degrees from the top, i.e. the  $6\ \mu\text{m}$  thick side. In simulations for the LHC environment and of neutron irradiations we assume an isotropic distribution, i.e. each event in the silicon is given a random orientation. Actually our simulations have shown that the orientation of the event is hardly noticeable in the predicted SEU cross section.

From each event only protons and heavier charged fragments are taken for transport. Because our considered silicon volume is very thin there is no need to consider further interactions of the produced fast secondaries with  $Z \leq 1$ .

We should point out that we have considered only interactions in silicon. In reality other materials, like  $\text{SiO}_2$  and some metals are also present in the close vicinity of the SV. For example, tungsten is often used to make the contact between silicon and the metal 1 layer. Silicon dioxide we can safely assume to be equivalent to silicon, but for heavy metals, like tungsten, this is not true. In fact we can get even fission events in tungsten and the emitted fragments typically have an atomic number of about 40 and an energy of 100 MeV. Compared to Si-ions these can give much higher energy depositions within the SV. We have studied the effect of the presence of tungsten close to the SV and indeed we found the expected very high energy depositions. However, due to the small amount of tungsten, the probability for such cases was very low and the SEU cross section was always dominated by the reactions in silicon. Nevertheless, the fission fragments from tungsten could play a role in Single Event Latchup studies, which are beyond the scope of this paper.

#### **4 Device characterization with heavy ions**

The SEU sensitivity of a circuit is most conveniently tested with heavy-ion irradiations. Dedicated facilities allow to irradiate a device with different ion types. Because each heavy ion has a characteristic LET the use of several ions allows to characterize the device. Usually the data are given as a function of LET and not  $E_{\text{dep}}$  as we prefer to do. In order to transform between these two we need to know or guess the sensitive depth of the device. A typical heavy-ion SEU cross section curve is shown in Fig. 4. We can observe a very sharp threshold below which the circuit does not upset. Above this threshold the upset rate first increases rapidly and then slowly saturates. This saturation corresponds to the situation where all sensitive regions of the device upset when hit by an ion so that a further increase of LET has no effect. The saturation value, divided by the number of sensitive nodes on the device, provides the cross sectional area of the sensitive region per node. This area multiplied by the thickness gives the sensitive volume

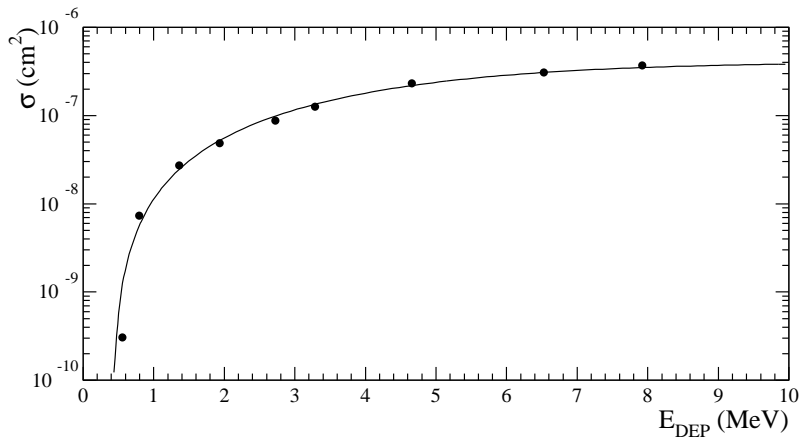


Fig. 4. Weibull fit to experimental heavy ion data for the AS5C4008CW-35E, 4Mbit SRAM from Austin [7]. We have assumed a sensitive depth of  $1 \mu\text{m}$  to convert from LET to  $E_{\text{dep}}$ .

(SV). It should be emphasized that the heavy ion irradiation does not give information about the integrity of the SV – it can be one single cell or consist of several smaller sub-cells.

The results of the heavy ion irradiation are most conveniently represented by a Weibull fit, which as a function of the deposited ionization energy  $E_{\text{dep}}$  has the form

$$\sigma = \sigma_0 \left( 1 - \exp \left\{ - \left[ \frac{E_{\text{dep}} - E_0}{W} \right]^s \right\} \right).$$

Here  $W$  and  $s$  are shape parameters,  $\sigma_0$  is the saturation value of the SEU cross section and  $E_0$  the SEU threshold. Thus there are four free parameters to be fitted.

## 5 Results

### 5.1 Upsets induced by high-energy hadrons

One common SEU testing method is the to irradiate a circuit with protons. We can use the available proton data to test our simulation method. For this purpose we have to perform our simulation for the proton energy used in the test.

Because the most abundant silicon isotope has equal number of protons and neutrons, it is isospin symmetric. Thus the major difference between a proton and a neutron irradiation is the Coulomb repulsion, which mainly decreases the inelastic cross section of the proton at low energies. At energies exceeding few tens of MeV there is no reason to expect significant differences for proton and neutron SEU rates.

Fig. 5 shows the simulated energy spectra of recoils for various incident neutron energies above 20 MeV. It can be seen that the change of model at  $E=20$  MeV introduces some discontinuity in particular predicts a lower probability for very high energy fragments. We will discuss this



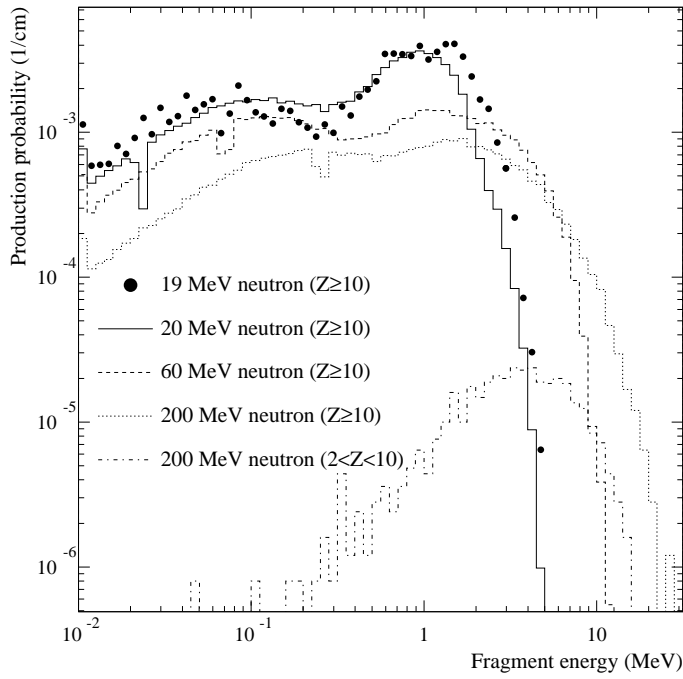


Fig. 5. Fragment energy spectra from  $n$ - $^{28}\text{Si}$  scattering at energies above 20 MeV. The inelastic fragments are generated with the event generators of the FLUKA code and the elastic ones with an optical model. For comparison the result from the low-energy model at 19 MeV is shown.

discrepancy in more detail in connection with low-energy neutrons. As expected the maximum energy of fragments increases with the energy of the incident neutrons. Below 60 MeV essentially all produced fragments have an atomic number ( $Z$ ) of at least 10 and thus have a  $dE/dx$  rather close to silicon. At 200 MeV a small fraction of the fragments have atomic number below 10.

In order to understand some general trends for different incident hadron types, energies and SV sizes, it is useful to first consider the most simple model where we assume that the SEU threshold would be a sharp step for a given SV size. In this case we assume that we have an upset if, and only if, the ionization within the SV exceeds  $E_{\text{crit}}$ . Only in this simple model the SEU cross section can be identified with the probability to have  $E_{\text{dep}} > E_{\text{crit}}$ . Fig. 6 shows such energy deposition probabilities in a SV of  $1 \times 1 \times 1 \mu\text{m}$  for four proton energies. At very low energies the probability increases with decreasing energy. This behaviour is consistent with the energy dependence of the p-Si total cross section. At  $E_{\text{crit}}$  of about 500 keV our simulations predict the same SEU rate for all studied proton energies. Thereafter the 20 MeV curve drops very rapidly, the 30 MeV curve is a bit shallower and high ends of the 60 MeV and 200 MeV curves are almost identical. This behaviour at high  $E_{\text{dep}}$  values is clearly due to the increasing maxima of fragment energies shown in Fig 5.

Fig. 6 suggests that the SEU cross section has a strong dependence on  $E_{\text{crit}}$ . The other important parameter is the size of the SV. In Fig. 7 we show how the SEU cross section varies as a function of  $E_{\text{crit}}$  and SV size. A particularly interesting feature is that the SEU cross section is almost

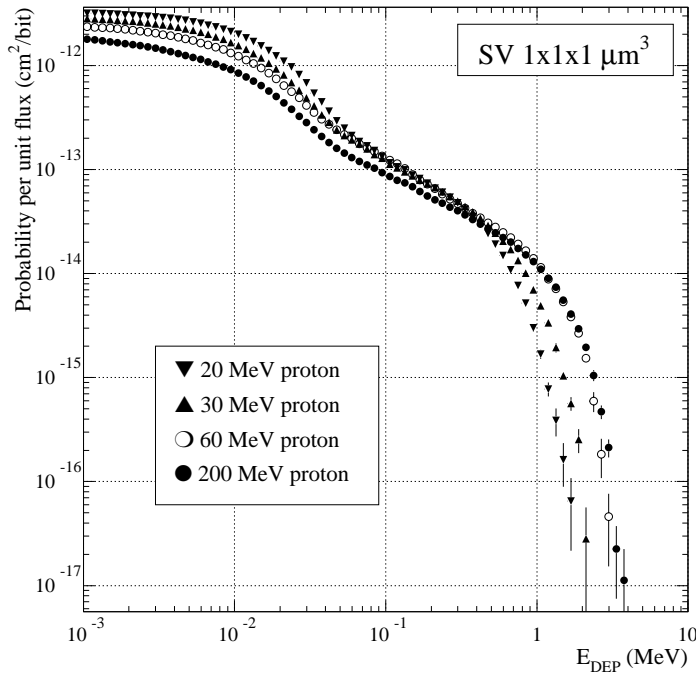


Fig. 6. Energy deposition probabilities for protons of different energies. The curve shows the probability to have within the SV an ionizing deposition greater or equal to the indicated  $E_{dep}$  value.

independent of the proton energy if  $E_{crit}$  is very low. Only for  $E_{crit} > 500$  keV a clear dependence on incident proton energy starts to show up. This energy dependence is not significantly affected by the SV size.

At first sight Fig. 7 seems to suggest that the SEU cross section is proportional to the volume of the SV. However, a simple volume argument does not explain why we find in Fig. 7 the largest SV size dependence for 20 MeV proton energy and  $E_{crit} = 1$  MeV. The true dependence on SV size actually is more complicated, because with increasing size of the SV both the probability of a path segment to cross the SV and the the maximum possible pathlength within the SV increase. The probability for a fragment to hit the SV is roughly proportional the cross sectional area of the SV. But in order to deposit enough energy the path-length within the SV must be long enough and this will be roughly proportional to the characteristic dimension of the SV. Thus, for a uniform  $dE/dx$  distribution of fragments, the SEU cross-section should be roughly proportional to the volume of the SV. But this picture is a bit too simplistic because in reality the probability of a fragment to hit the SV depends also on its range, the  $dE/dx$  distribution is not uniform, some fragments are produced within the SV and some have a range shorter than the SV dimensions. For recoils produced by 20 MeV protons these latter aspects become important. From Fig. 5 we can see that the fragment distribution drops rapidly above 1 MeV. According to Fig. 3 the energy deposited by such fragments can barely exceed  $E_{crit}=1$  MeV and thus the pathlength within the SV plays a significant role. At higher incident energies the recoil spectrum is flatter and reaches to higher energies which means that the  $dE/dx$  distribution is more uniform and extends to higher values. Thus our arguments that the SEU cross section is proportional to the SV size are better valid at high energies.

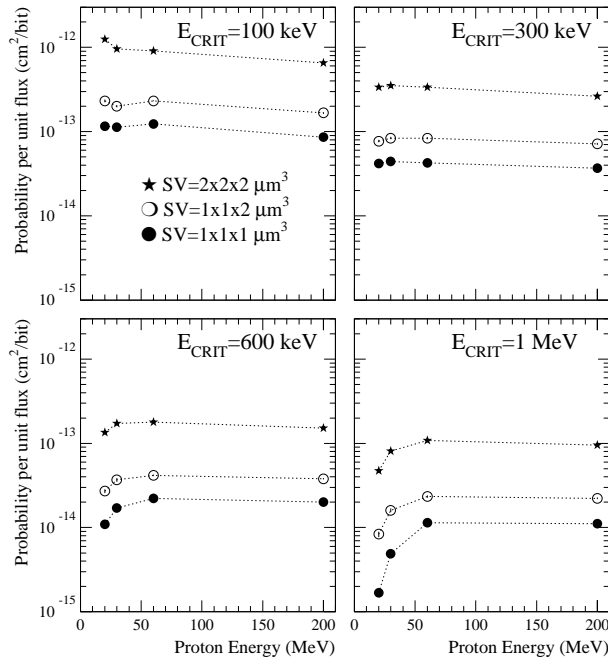


Fig. 7. Variation of the SEU cross section as a function of  $E_{\text{crit}}$  and SV size assuming a step-like SEU threshold at  $E_{\text{crit}}$ . The statistical error bars are smaller than the symbol sizes.

## 5.2 Upsets induced by neutrons below 20 MeV

We next have to consider neutron reactions in the silicon itself. In doing so, we will consider only  $^{28}\text{Si}$  and neglect the two isotopes  $^{29}\text{Si}$  and  $^{30}\text{Si}$  although they have a non-negligible natural abundance. Since the cross sections and reaction thresholds of these isotopes are very similar to those of  $^{28}\text{Si}$ , their inclusion should not have any effect on our results.

Whereas the average fragment energies increase quite smoothly above 10 MeV the situation is quite different at lower energies. This is illustrated in Fig. 8 where it can be seen that the maximum fragment energies very quickly decrease when the incident neutron energy falls below 10 MeV. The threshold for  $(n,n')$  scattering in  $^{28}\text{Si}$  is 1.8 MeV. Essentially all scattering below this energy is elastic. At 2 MeV the inelastic component is still negligible and indeed we observe the highest fragment energies at just below 300 keV which agrees very well with the maximum energy transfer in elastic n-Si scattering. Because SEU will usually require an  $E_{\text{dep}}$  of at least few hundred keV, we do not expect to see upsets below 2 MeV of neutron energy – except for a possible effect of thermal neutrons.

Fig. 5 already indicated that there is some discrepancy in the recoil energy at 20 MeV where we join our low-energy and high-energy fragment generation models. We have calculated the  $E_{\text{dep}}$  probabilities with both models at 20 MeV and the comparison is shown in Fig. 9. FLUKA clearly predicts a lower probability for high  $E_{\text{dep}}$ . The most energetic fragments are produced when the residual recoils against an emitted  $\alpha$  and indeed we have traced the difference back to a lower  $\alpha$  production cross section in FLUKA – 63 mb against 214 mb in ENDFB-VI. In

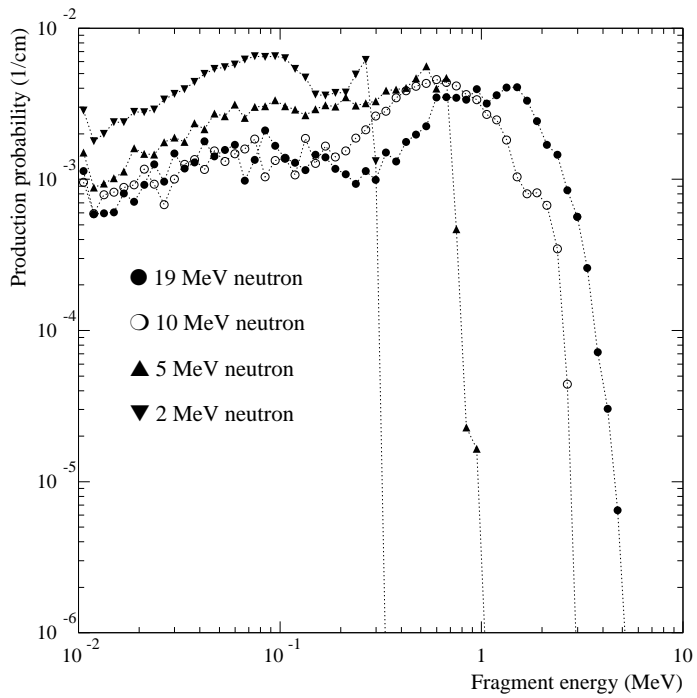


Fig. 8. Fragment energy spectra from  $n\text{-}^{28}\text{Si}$  scattering at low energies. The spectra are based on direct sampling from ENDFB-VI data for  $^{28}\text{Si}$ .

Fig. 9 we verify that most of the depositions exceeding 1 MeV in the SV are due to  $(n,\alpha)$ -reactions and in particular the emitted magnesium recoil. The difference between our energy deposition probabilities at 20 MeV is fully explained by the deficiency of  $(n,\alpha)$  reactions in the FLUKA model. We conclude that the FLUKA model starts to fail at these low energies and it is preferable to use the ENDFB-VI data up to the highest energy available (20 MeV).

Fig. 10 shows the  $E_{\text{dep}}$  probabilities of 3.1 MeV and 14 MeV neutrons for two different SV sizes. A very significant difference can be observed between the two energies: while the shape of the 14 MeV curve resembles that of the high energy proton curves the 3.1 MeV probability drops to zero at about 300 keV. This is consistent with the recoil spectra shown in Fig. 8. If we consider elastic scattering of 3.1 MeV neutrons, the maximum energy transfer is about 410 keV for which Fig. 3 indicates an ionization of 200 keV. Some larger energy transfers come from  $(n,n')$  scattering which has a threshold at 1.8 MeV and in addition we observe a high energy tail which is completely explained by  $(n,\alpha)$  reactions. Fig. 10 indicates that if a device has  $E_{\text{crit}} > 200$  keV, neutrons below 2 MeV of energy will not contribute to the SEU rate – with the exception of the possible  $^{10}\text{B}(n,\alpha)^7\text{Li}$  reaction to be discussed below.

### 5.3 Upsets induced by thermal neutrons

It has been recently shown that at least some devices can upset when exposed to thermal neutrons [8]. Although such reactions are not expected to be the most important source of SEU at LHC we consider this reaction for completeness. It also represents a particularly simple case

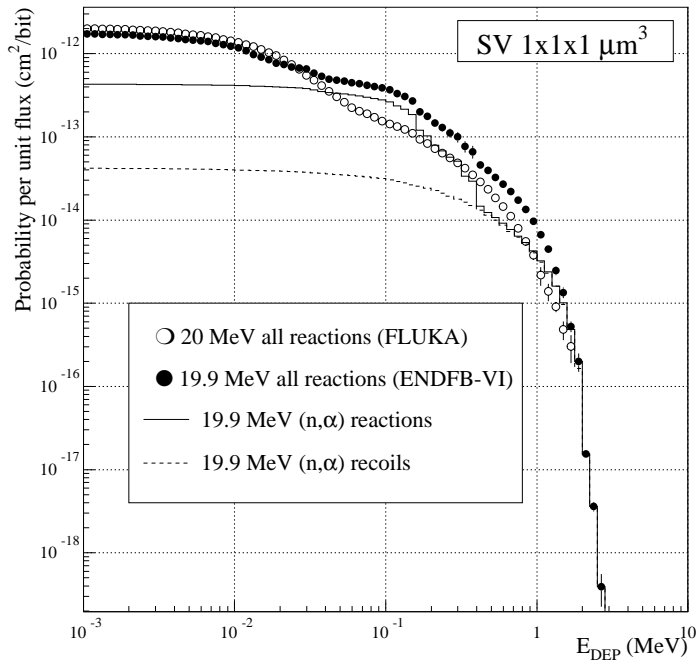


Fig. 9. Energy deposition probabilities for neutrons at 20 MeV where low- and high-energy models join. The importance of (n,α) reactions (solid line) and especially the Mg-recoil emitted in these reactions (dashed line) is emphasized.

because there are only four discrete fragment energies.

Boron, which is a common dopant in the manufacture of ICs, introduces the isotope  $^{10}\text{B}$ . This has a 3.8 kb thermal cross section for the reaction  $^{10}\text{B}(n,\alpha)^7\text{Li}$  which releases 2.8 MeV of energy. In most cases the energy is shared between a 478 keV photon and the two fragments. The resulting energies are 1.47 MeV for the  $\alpha$  and 0.84 MeV for the  $^7\text{Li}$ . Potentially more significant are the 6% of cases where no photon is emitted. In this case the recoil energies are 1.79 MeV and 1.01 MeV, respectively. From Fig. 1 we can see that both fragments can deposit a few hundred keV per micron of path-length. This certainly can exceed the critical energies of some circuits.

The problem in considering thermal neutron induced SEU is that the boron concentration and distribution is not known and the SEU rate will depend linearly on this. Thus no real quantitative estimates are possible. We include this reaction in our simulations with a guessed uniform boron concentration of  $10^{17}$  atoms per cubic centimetre. The resulting energy deposition probabilities are shown in Fig. 11.

If we consider that both the  $\alpha$  and the  $^7\text{Li}$  are produced with about 1 MeV of energy we see from Fig. 2 that they have a range of about  $3\ \mu\text{m}$ . Thus both considered SV sizes are small enough to restrict the energy deposition. This range also indicates that the boron concentration beyond  $3\ \mu\text{m}$  from the SV boundary does not play any role.

A comparison of the two sensitive volumes shown in Fig. 11 illustrates an interesting difference to the high-energy interactions, where a continuous distribution of fragment energies, i.e.  $dE/dx$  values, caused the SEU cross section to be proportional to the SV. With discrete energies,

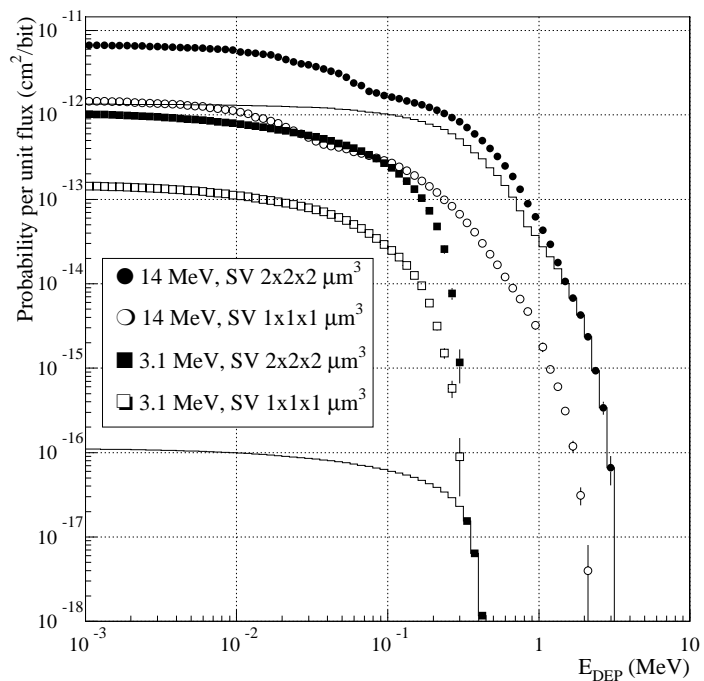


Fig. 10. Energy deposition probabilities for 3.1 MeV and 14 MeV neutrons with two different SV sizes. The solid lines show the contribution of  $(n,\alpha)$  reactions for the  $2 \times 2 \times 2 \mu\text{m}^3$  cases.

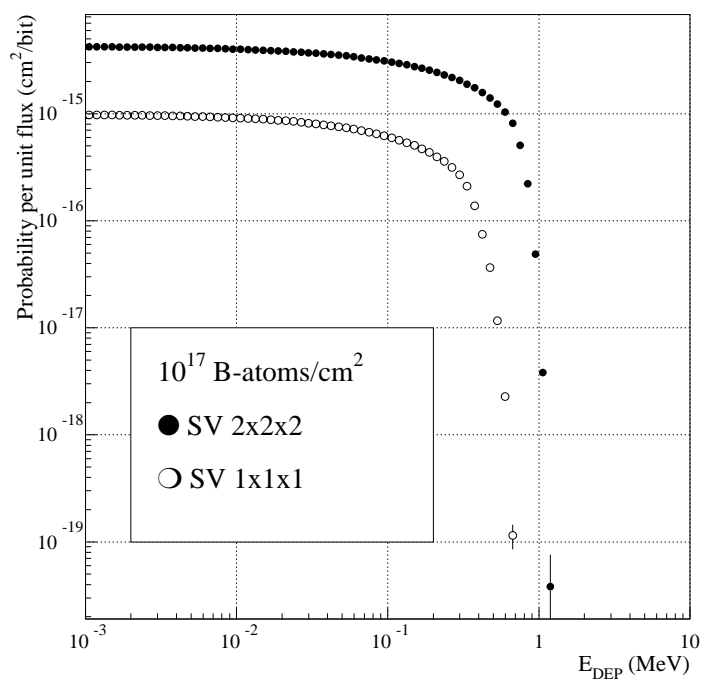


Fig. 11. Energy deposition probabilities for the thermal neutron reaction  $^{10}\text{B}(n,\alpha)^7\text{Li}$  for two different SV sizes and a guessed uniform boron concentration.

corresponding to  $E_{\text{dep}}$  well above  $E_{\text{crit}}$  the pathlength is insignificant and the device is sensitive to each fragment hitting the SV. Thus the probability should be roughly proportional to the cross sectional area of the SV and indeed we observe a factor of about 4 difference between  $1 \times 1 \times 1 \mu\text{m}^3$  and  $2 \times 2 \times 2 \mu\text{m}^3$ . With increasing  $E_{\text{crit}}$  – when the  $E_{\text{dep}}$  probability turns to a rapid fall – it becomes increasingly important to contain as much as possible of the  $3 \mu\text{m}$  long path of the fragment within the SV and we observe an increasing difference between the two SV sizes. Ultimately the two curves drop to zero about a factor of 2 apart in terms of  $E_{\text{dep}}$ , corresponding to the difference in the largest possible pathlength within the SV.

We should also point out that for simplicity we consider only the thermal ( $n, \alpha$ ) cross section of  $^{10}\text{B}$  and apply it to the flux in the thermal group of FLUKA, which represents the average spectrum up to 0.414 eV. Actually the cross section decreases gradually towards higher energies which means that, depending on the shape of the spectrum, we might slightly underestimate the upset rate.

## 6 Comparison with experimental results

### 6.1 Protons

Our simplistic model with a step-like critical energy and a fixed size SV is not very realistic and we can significantly improve by using a Weibull fit to actual heavy-ion data of the device to be studied [9]. For each energy bin  $i$  we have from Fig. 6 the energy deposition probability  $P_i$  and can calculate from the Weibull distribution the increase of sensitive area in this energy interval:  $\Delta\sigma_i = (\sigma_{i+1} - \sigma_i)/\sigma_0$ . We can then derive the SEU cross section  $\Sigma$  in the proton environment as

$$\Sigma = \sum_i P_i \Delta\sigma_i \frac{\sigma_0}{A},$$

where  $A$  is the cross sectional area of the SV used in our simulation. Results of such a calculation are compared to experimental data in Table 1.

From the values in Table 1 we can see a systematic dependence of our estimate as a function of the shape and size of the SV. When the SV decreases our estimate always increases. This can be understood from Fig. 3, where we can see that most fragments will not have reached the saturation value of energy loss and therefore have their largest loss at the beginning of their path. Therefore the energy deposition per unit of volume increases when we decrease the SV. At the same time a decreasing sensitive depth means that the threshold of our Weibull fit moves towards a lower  $E_{\text{dep}}$  value. But for a cubic SV this latter effect is roughly compensated because the average pathlength of most fragments within the SV decreases pro-rata.

The dependence on the shape of the SV is more dramatic. If we assume a flat SV, i.e. a small sensitive depth and a large area, the threshold of the Weibull function decreases, but the average pathlength of an isotropic fragment flux does not follow pro-rata. Thus a flat SV always leads to a significant increase of our estimate. However, this increase will not be unlimited, because fragment ranges and the thinnest dimension of the SV will limit the maximum pathlengths. The opposite effect is observed when we assume a deep SV, i.e. one where the cross sectional area is

Device	SA	Experimental	$1 \times 1 \times 0.5$	$1 \times 1 \times 1$	$1 \times 1 \times 2$	$2 \times 2 \times 2$
Fairchild 2901B $\mu$ P 4 bit slice	3750	$8.5 \times 10^{-10}$	$1.0 \times 10^{-9}$	$5.2 \times 10^{-10}$	$1.8 \times 10^{-10}$	$3.7 \times 10^{-10}$
Hitachi HM6116 SRAM 2K*8	403	$4.6 \times 10^{-8}$	$2.3 \times 10^{-8}$	$9.6 \times 10^{-9}$	$2.6 \times 10^{-9}$	$6.3 \times 10^{-9}$
Hitachi 62256R 256K SRAM	244	$1.5 \times 10^{-7}$	$1.6 \times 10^{-7}$	$1.0 \times 10^{-7}$	$5.2 \times 10^{-8}$	$8.0 \times 10^{-8}$
Harris HM6516 SRAM 2K*8	183	$2.5 \times 10^{-9}$	$4.2 \times 10^{-9}$	$1.6 \times 10^{-9}$	$4.0 \times 10^{-10}$	$1.0 \times 10^{-9}$
OmniWawe OW_62256 SRAM 32K*8	164	$8.7 \times 10^{-8}$	$7.5 \times 10^{-8}$	$3.6 \times 10^{-8}$	$1.3 \times 10^{-8}$	$2.5 \times 10^{-8}$
Fujitsu MB814100-10PSZ 4Mx1 DRAM	76.3	$6.9 \times 10^{-7}$	$1.6 \times 10^{-6}$	$1.3 \times 10^{-6}$	$8.3 \times 10^{-7}$	$1.1 \times 10^{-6}$
Toshiba TC514100Z-10 4Mx1 DRAM	50.1	$1.0 \times 10^{-6}$	$1.2 \times 10^{-6}$	$9.8 \times 10^{-7}$	$7.4 \times 10^{-7}$	$8.9 \times 10^{-7}$
Siemens HYB514100J-10 4Mx1 DRAM	50.1	$1.5 \times 10^{-6}$	$1.6 \times 10^{-6}$	$1.3 \times 10^{-6}$	$1.0 \times 10^{-6}$	$1.2 \times 10^{-6}$
Texas Inst. SMJ44100 4Meg DRAM	47.7	$7.0 \times 10^{-7}$	$1.1 \times 10^{-6}$	$8.4 \times 10^{-7}$	$5.6 \times 10^{-7}$	$7.3 \times 10^{-7}$
Matra MHS HM_65656 SRAM 32K*8	42.0	$3.0 \times 10^{-8}$	$5.3 \times 10^{-8}$	$3.5 \times 10^{-8}$	$1.9 \times 10^{-8}$	$2.8 \times 10^{-8}$
Hitachi 62832H 256K SRAM	38.1	$2.9 \times 10^{-8}$	$1.8 \times 10^{-8}$	$9.5 \times 10^{-9}$	$3.6 \times 10^{-9}$	$7.0 \times 10^{-9}$
NEC D424100V-80 4Mx1 DRAM	35.8	$1.8 \times 10^{-6}$	$1.5 \times 10^{-6}$	$1.3 \times 10^{-6}$	$1.1 \times 10^{-6}$	$1.2 \times 10^{-6}$
Micron MT4C4001 DRAM 4Meg	31.0	$2.9 \times 10^{-7}$	$5.1 \times 10^{-7}$	$3.9 \times 10^{-7}$	$2.5 \times 10^{-7}$	$3.3 \times 10^{-7}$
Micron MT4C1004C 4Mx1 DRAM	31.0	$3.9 \times 10^{-7}$	$5.8 \times 10^{-7}$	$4.1 \times 10^{-7}$	$2.4 \times 10^{-7}$	$3.4 \times 10^{-7}$
Samsung KM41C4000Z-8 4Mx1 DRAM	31.0	$3.3 \times 10^{-7}$	$4.5 \times 10^{-7}$	$3.1 \times 10^{-7}$	$1.8 \times 10^{-7}$	$2.6 \times 10^{-7}$
IBM 01G9274 DRAM 4 Meg	2.31	$4.2 \times 10^{-9}$	$2.8 \times 10^{-9}$	$9.3 \times 10^{-10}$	$2.8 \times 10^{-10}$	$6.1 \times 10^{-10}$
IBM LUNA_C 16Meg DRAM	0.89	$2.1 \times 10^{-8}$	$2.1 \times 10^{-8}$	$7.0 \times 10^{-9}$	$1.8 \times 10^{-9}$	$4.5 \times 10^{-9}$
IBM_16Meg 16Meg DRAM	0.77	$2.1 \times 10^{-8}$	$1.2 \times 10^{-8}$	$4.4 \times 10^{-9}$	$1.4 \times 10^{-9}$	$3.0 \times 10^{-9}$
Minimum Predicted/Experimental			0.50	0.21	0.057	0.14
Maximum Predicted/Experimental			2.3	1.9	1.2	1.6
Average Predicted/Experimental (rms %)			1.2 (9.5%)	0.77 (14%)	0.44 (17%)	0.63 (15%)

Table 1  
Experimental 200 MeV proton SEU cross sections (in  $\text{cm}^2$ ) and our calculated values for various SV sizes. SA gives the sensitive area in  $\mu\text{m}^2$  per bit. Experimental data and Weibull parameters are from [10].



Device	Experimental	$1 \times 1 \times 0.5$	$1 \times 1 \times 1$	$1 \times 1 \times 2$	$2 \times 2 \times 2$
M5M5408_B	$2.5 \times 10^{-13}$	$4.3 \times 10^{-13}$	$2.1 \times 10^{-13}$	$5.0 \times 10^{-14}$	$1.2 \times 10^{-13}$
IDT71256	$2.7 \times 10^{-14}$	$1.1 \times 10^{-13}$	$3.4 \times 10^{-14}$	$3.8 \times 10^{-15}$	$1.3 \times 10^{-14}$
MCM6246	$8.2 \times 10^{-15}$	$1.7 \times 10^{-14}$	$3.1 \times 10^{-15}$	$8.1 \times 10^{-17}$	$6.5 \times 10^{-16}$
MHS65608E	$3.3 \times 10^{-14}$	$3.4 \times 10^{-14}$	$1.1 \times 10^{-14}$	$1.2 \times 10^{-15}$	$3.9 \times 10^{-15}$
Minimum Predicted/Experimental		1.0	0.33	0.0099	0.079
Maximum Predicted/Experimental		4.1	1.3	0.20	0.48
Average Predicted/Experimental		2.2	0.70	0.098	0.29

Table 2

Experimental 14 MeV neutron SEU cross sections (in  $\text{cm}^2/\text{bit}$ ) and our calculated values for various SV sizes. Experimental data are from [9,11].

smaller than the depth. In this case the Weibull threshold moves to higher energies which leads to a decrease of our estimate.

In Table 1 the overall error is minimized for the  $1 \times 1 \times 0.5 \mu\text{m}$  SV – we not only center the Predicted/Experiment ratio close to unity, but also its spread is minimized. The implication appears to be that the SV of most devices tends to be rather flat than cubic. This does not appear unreasonable if we consider the surface areas in Table 1 which, except for the IBM devices, are several tens of  $\mu\text{m}^2$ . Although this is the most likely explanation, we must also consider that by using a flat SV we bias our prediction by imposing the claim that the heavy ion traverses the thinnest dimension of the SV. Thus we in some sense, via the aspect ratio of the SV, make the threshold of the Weibull function a tunable parameter, which of course is not a desired feature in a predictive model. We also should point out that we made calculations also for a very large flat SV of  $3 \times 3 \times 1 \mu\text{m}^3$  and found that our estimates were systematically – although very slightly – lower than for the smaller  $1 \times 1 \times 0.5 \mu\text{m}^3$  volume. Purely from the aspect ratio argument one would have expected the opposite but the expected increase is probably compensated by the tendency of our estimate to systematically decrease with increasing SV.

From the comparison of the results obtained with different SV size and shape, it appears that the best approach is to use either the  $1 \times 1 \times 1 \mu\text{m}^3$  SV or the  $1 \times 1 \times 0.5 \mu\text{m}^3$  SV for all devices.

### 6.1.1 Neutrons 2–20 MeV

Because neutrons are known to be an important component of the radiation field at hadron accelerators it is imperative that we confront our simulations also with some neutron upset data. Unfortunately such data – we need both neutron and heavy-ion upset measurements for the same device – are much more scarce than for protons so that our sample is not very representative.

Table 2 shows the comparison of our calculations with the few experimental neutron data which were available to us. In addition we had some data for 3.1 MeV neutrons but here both simulations and data showed no upsets.

At 14 MeV neutron energy the agreement between our simulation and experiment is not as good as for 200 MeV protons. In particular we observe a much more significant dependence on the

Particle	Direction	Total	Elastic
10 GeV proton	beam	1.2	0.006
200 MeV proton	beam	1.0	0.011
200 MeV neutron	beam	0.97	0.007
200 MeV pion	beam	2.0	0.012
60 MeV proton	beam	1.05	0.028
20 MeV proton	beam	0.45	0.10
20 MeV neutron	beam	0.46	0.022
200 MeV proton	isotropic	1.03	0.010
20 MeV neutron	isotropic	0.43	0.021
19.9 MeV neutron	isotropic	0.92	0.099
14 MeV neutron	isotropic	0.44	0.041
3.1 MeV neutron	isotropic	$2 \times 10^{-7}$	—

Table 3

SEU cross sections relative to the cross section of 200 MeV protons ( $2.0 \times 10^{-13}$  cm<sup>2</sup>/bit) in the Texas Instruments SMJ44100 4Meg DRAM assuming a  $1 \times 1 \times 1$   $\mu$ m SV.

size of the SV. Contrary to the 200 MeV case the effect of the sensitive depth does not seem to cancel out for low-energy neutrons. The reason is that a change of the sensitive depth directly moves the threshold of the Weibull curve, expressed in terms of  $E_{\text{dep}}$ . In the 200 MeV case with a fragment distribution ranging to high energies, this was compensated by the increased range of the fragments. However, from Fig. 8 we can see that for low-energy neutrons the fragment energy distribution drops very rapidly at relatively low energies. The range of these fragments is so short that an increase of the SV size does not increase the energy deposition significantly. Thus a rather accurate guess of the sensitive depth is needed to predict reliable results for low energy neutrons.

In this context we would like to point out that many other models to simulate SEU rates use the concept of a critical LET instead of  $E_{\text{crit}}$  to determine the onset of SEU. These methods do not explicitly encounter the uncertainty of the sensitive depth. However, they implicitly have the analogous – and in fact more severe – uncertainty that the path length and the variation of dE/dx inside the SV is not considered at all. In the limit of going to a very small SV our method becomes equivalent to using a critical LET.

## 7 Comparison of SEU cross section for different radiation types

We have chosen the SMJ44100 4Meg DRAM from Texas Instruments as an example device to study upset rates in various environments. Table 3 shows the simulated SEU rates for this chip in different irradiation conditions. We can make several interesting observations:

- (1) As expected neutrons and protons of the same energy produce almost identical upset rates if the incident energy exceeds 20 MeV.
- (2) The discrepancy between our two models at 20 MeV is reflected in the upset rate. There is an even larger discrepancy in the upset rate due to elastic collisions, but this is not surprising because for 20 MeV neutrons we have pushed the Glauber optical model below its range of validity.
- (3) For all particles and energies elastic scattering gives a negligible, or at most minor, contribution to the SEU rate.
- (4) The upset rate for 10 GeV protons is only slightly higher than for 200 MeV protons. This seems reasonable, because an increase of energy should not significantly increase the recoil energy in peripheral collisions. In central collisions at high energy the target is likely to break into small pieces which have lower LET.
- (5) For 200 MeV pions we observe twice the upset rate of protons of the same energy. This corresponds to a 20% excess over the ratio of inelastic cross sections.
- (6) Our simulations for isotropic and monodirectional (beam) irradiation show negligible impact on the SEU rate. This is found to be true also for a non-cubic SV.

## 8 SEU predictions for the LHC environment

It first should be strongly emphasized that we are not able to predict SEU rates for final LHC electronics because some of the devices have not even been chosen yet and of the chosen none has been so far characterized in a heavy-ion beam.

However, it is certainly useful to have some rough indication of the possible upset rates. These we can obtain by performing our simulations with the predicted LHC hadron spectrum for some circuit where heavy-ion data exists and which we consider somehow representative of LHC electronics.

For this example study we use spectra in various parts of the CMS experiment. These should be fairly representative also for other LHC detectors when properly scaled with the corresponding hadron fluence.

In CMS the composition and intensity of the radiation field is a strong function of the position. Already within the inner tracker, which extends to a radius of 1.2 m inside a solenoidal 4 T field, we encounter quite different compositions of the hadron flux. The pixel detector very close to the beam pipe is exposed to an intense hadron flux which is mostly composed of pions. The expected fluence is about  $2 \times 10^{15} \text{ cm}^{-2}$  over ten years of operation. At the outer periphery the charged hadron flux is significantly reduced and neutrons emitted from the surrounding  $\text{PbWO}_4$  electromagnetic calorimeter (ECAL) dominate. The fluence is about two orders of magnitude lower than at the pixel detector. Behind the ECAL we find a neutron environment with only about 10% other hadrons. The 10-year fluence ranges from  $1 \times 10^{13} \text{ cm}^{-2}$  behind the barrel ECAL to  $2 \times 10^{14} \text{ cm}^{-2}$  at the high-rapidity edge of the endcap.

Finally, in the underground experimental cavern where power supplies and control electronics will be positioned essentially all of the hadron radiation consists of neutrons. The design goal for shielding is to keep the total fluence below  $10^{11} \text{ cm}^{-2}$  over 10 years.

	Pixel detector $\eta=0-0.9$ R=4–20 cm	Outer Tracker $\eta=0-0.9$ R=65–120	Behind Endcap ECAL R=50–130	Expt. Cavern above endcap R=700-1200
Protons	$2.3 \times 10^6$	22000	30000	1.6
Pions	$1.1 \times 10^7$	68000	68000	0.035
Thermal neutron	$9.9 \times 10^5$	$9.5 \times 10^5$	$1.8 \times 10^6$	370
Neutron E=2-20 MeV	$5.6 \times 10^5$	76000	$1.4 \times 10^5$	93
Neutron E>20 MeV	$1.0 \times 10^6$	60000	$2.0 \times 10^5$	84
Neutron total	$3.0 \times 10^6$	$1.4 \times 10^6$	$2.9 \times 10^6$	1100

Table 4

Hadron fluxes in various parts of the CMS experiment. The flux of Kaons and other heavier hadrons is counted with the protons. The last line includes all neutrons from thermal to the maximum energy. All values given per  $\text{cm}^2$  per second at LHC peak luminosity.

As we have shown above we have to divide the flux into three groups: thermal neutrons which we need to consider only for the  $^{10}\text{B}(n,\alpha)^7\text{Li}$  reaction, 2–20 MeV neutrons, where the lower limit corresponds to the threshold of inelastic reactions in silicon and fast hadrons. The last group includes all charged hadrons with their energy exceeding the Coulomb barrier, and neutrons above 20 MeV. Inside these regimes –except the thermal one – we of course consider the detailed spectrum.

Such a division is useful to introduce because it allows a more reliable scaling of our results with just the total flux within each energy regime. We have shown with our proton studies that above few tens of MeV the SEU cross section is almost independent of the particle spectrum. Table 3 suggest that – possibly with the exception of pions – there is no significant variation due to hadron species either. The SEU sensitivity to neutrons varies quite a lot between 2 MeV and 20 MeV, but here the scalability of our results can be based on the fact that most spallation spectra usually have a rather similar shape in this energy range.

For charged hadrons the lower cutoff is not important, because the flux decreases rapidly with energy. We use a lower cutoff of 5 MeV, which roughly corresponds to the Coulomb barrier for positive hadrons. For negative pions this cutoff is not applied but no detailed analysis of pion stopping is performed. Thus possible SEU triggered by stopped negative pions is only approximately included. This contribution, however, should be negligible in all regions.

Table 4 shows the particle fluxes in our energy regimes in four regions of the CMS experiment. It should be emphasized that the spectrum of low energy neutrons depends strongly on the local material composition. In particular the presence of hydrogen or isotopes with large thermal neutron capture cross section can influence the spectrum significantly. These material effects become increasingly important towards lower energies and thus affect mainly the ratio of thermal to total neutron flux.

The spectra from which the values in Table 4 have been extracted are shown in Fig. 12. We can observe that the shape of the charged hadron spectrum remains almost invariant when we move from the immediate vicinity of the vertex to the outer periphery of the experimental cavern. But

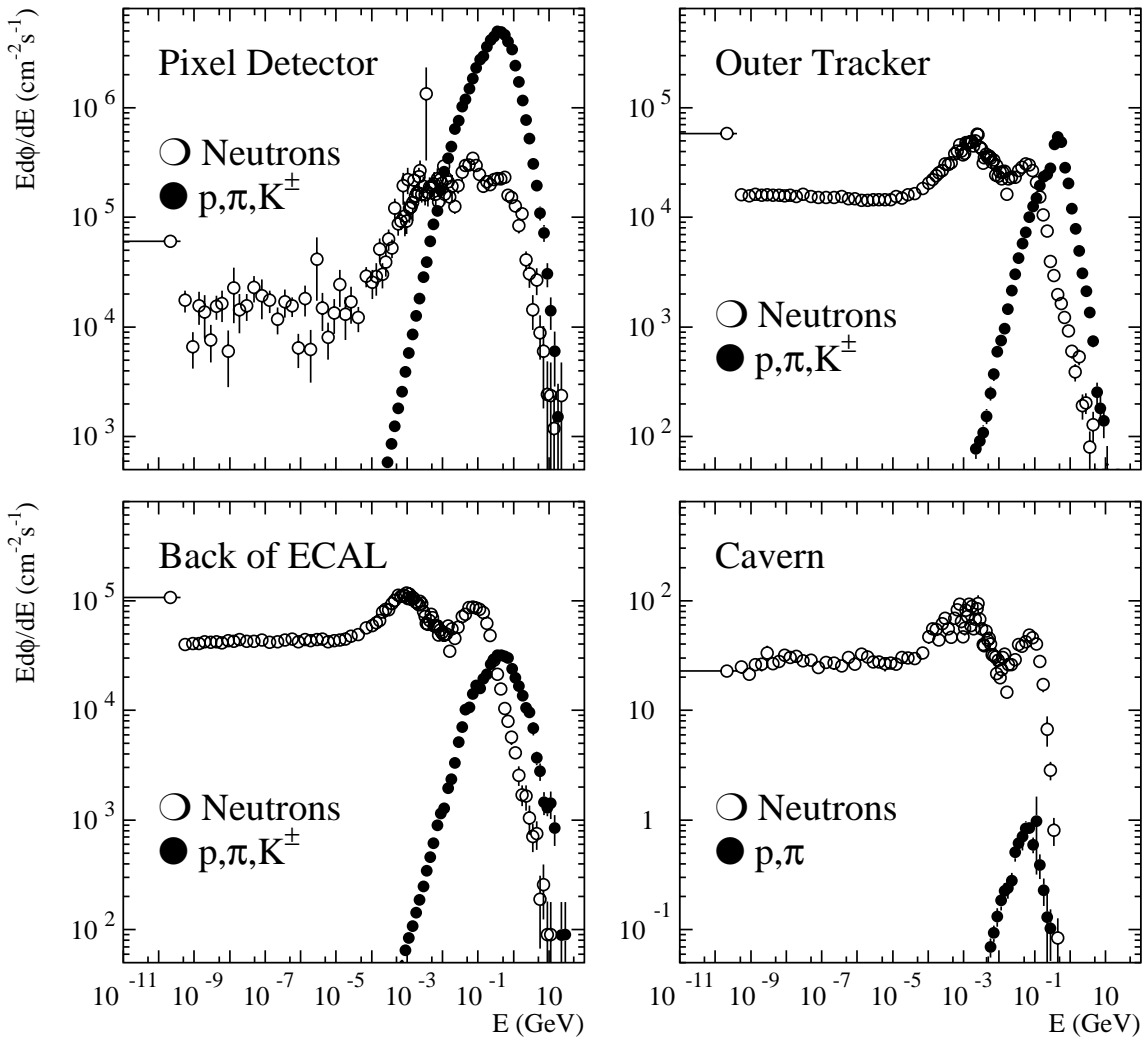


Fig. 12. Energy spectra of neutrons and charged hadrons in some regions of CMS in which significant amounts of electronics will be situated.

the absolute flux changes by 6 orders of magnitude. For the neutron flux the situation is quite different and we observe a significant position dependence of the neutron spectrum. It should be remarked that all spectra selected for Fig. 12 have a substantial low-energy component. This is fairly typical for all regions where electronics is situated, but there are other regions in CMS, particularly inside some calorimeters and steel structures, where the low-energy neutron flux can be several orders of magnitude below the peak at 1 MeV. Due to this variation the total neutron flux would not be a good quantity to scale predicted upset rates. This uncertainty is significantly reduced when we apply our cuts of 2 MeV and 20 MeV to the neutron spectrum.

Table 5 summarizes our predictions of the SEU cross sections for the SMJ44100 chip assuming a  $1 \times 1 \times 1 \mu\text{m}^3$  SV. This DRAM has a rather low  $E_{\text{crit}}$  of just above 300 keV. If we multiply the upset cross section with the corresponding fluxes from Table 4 we obtain the predictions for the upset rate per second and per bit which are also given in Table 5. We can see that the high energy hadrons always dominate the upset rate. The contribution from low-energy neutrons is

Region	>20 MeV hadrons		2–20 MeV neutrons		Thermal Neutrons
	$\Sigma$ (cm <sup>2</sup> )	$\phi \times \Sigma$	$\Sigma$ (cm <sup>2</sup> )	$\phi \times \Sigma$	$\phi \times \Sigma$
Pixel detector	$3.1 \times 10^{-13}$	$4.4 \times 10^{-6}$	$2.6 \times 10^{-14}$	$1.5 \times 10^{-8}$	$1.3 \times 10^{-10}$
Outer tracker	$2.6 \times 10^{-13}$	$3.9 \times 10^{-8}$	$2.5 \times 10^{-14}$	$1.9 \times 10^{-9}$	$1.3 \times 10^{-10}$
Behind Endcap	$2.1 \times 10^{-13}$	$6.3 \times 10^{-8}$	$2.9 \times 10^{-14}$	$4.1 \times 10^{-9}$	$2.4 \times 10^{-10}$
Expt. Cavern	$1.7 \times 10^{-13}$	$1.5 \times 10^{-11}$	$1.7 \times 10^{-14}$	$1.6 \times 10^{-12}$	$5.0 \times 10^{-14}$

Table 5

SEU cross sections per bit ( $\Sigma$ ) and upset rates per bit per second ( $\phi \times \Sigma$ ) for a SMJ44100 4Meg DRAM chip if it would be positioned in different parts of CMS. For fluxes see Table 4. For thermal neutrons we assume a boron concentration of  $10^{17} \text{ cm}^{-3}$  which gives a SEU cross section of  $1.3 \times 10^{-16} \text{ cm}^2/\text{bit}$ .

about an order of magnitude smaller in all regions of CMS. It should of course be pointed out that our thermal neutron estimate could be higher if our guess of  $10^{17} \text{ cm}^{-3}$  for the boron doping is too low. It seems unlikely, however, that it would become comparable to the high-energy hadrons since this would require boron concentrations of almost  $10^{20} \text{ cm}^{-3}$ , averaged over a few micrometres around the SV.

It should be remarked that the variation of the SEU cross section for 2–20 MeV neutrons is less than a factor of 2. This means that small variations of the spectrum are not important and upset rates scale with the energy-integrated flux. From Table 5, excluding the pixel detector, we can determine the average SEU cross section for high-energy hadrons at LHC to be about  $2 \times 10^{-13} \text{ cm}^{-2}$  and an order of magnitude less for 2–20 MeV neutrons.

A total upset rate of about  $2 \times 10^{-11} \text{ s}^{-1}$  per bit – as we find for the cavern – appears small but if we assume that in 10 years the LHC will operate for  $5 \times 10^7$  seconds of peak luminosity equivalent, there would still be 4000 upsets in the full 4 Mbit chip over 10 years. With 180 days operation per year this corresponds to about two upsets per day in each chip of this type. At the level of the pixel detector the particle flux is orders of magnitude higher, leading to a rate of about 200 upsets per bit in 10 years. We should also point out that this is the average rate over the whole pixel detector. The flux – and thus the upset rate – at the innermost layer is about a factor of 3 larger than this average.

We should re-emphasize that our example SMJ44100 chip is not a realistic representation of the front-end electronics of the innermost detectors. We only have used it to illustrate our method and to give an idea of the variation of upset rates as a function of position within CMS.

The average SEU cross sections obtained for the LHC-spectra are almost the same as those given for protons in Table 3. Thus an irradiation in a proton beam of 60-200 MeV should provide a good means to test LHC electronics components for SEU-sensitivity. On the other hand an irradiation with low-energy neutrons does not seem a suitable SEU testing method for LHC applications. In particular we want to strongly emphasize that the concept of 1 MeV neutron equivalent, which is commonly used to express hadron exposure of silicon devices, is meaningful only to in the context of bulk-damage and would be completely inappropriate for SEU studies.

One restriction to the use of fairly low energy protons is their short range. The dE/dx of 60 MeV

protons in silicon is roughly 20 MeV/cm and the range is slightly more than 1 cm. In typical plastic the range is almost 3 cm. Since the SEU cross section is roughly constant down to 30 MeV typical electronics packaging should not substantially affect the measured SEU rate. Dilution due to scattering might be more of a problem if the beam traverses material – including air – far upstream of the chip under test.

## 9 Limits of the model and sources of uncertainty

Despite the use of the Weibull fit the determination of the SV size and shape and of the critical energy remains as a major uncertainty in our simulation. The heavy ions probe the device only in one dimension, thus they essentially measure the cross sectional area of the SV. A determination of the critical energy requires an educated guess of the depth of the sensitive layer. Fortunately this is in most cases partly compensated by the fact that a smaller depth implies a smaller SV and thus a lower energy deposition probability. An additional drawback of the use of the Weibull curve is that in most cases we are very sensitive to the shape of the curve close to threshold, where the fit quality often is not very good.

All our simulations are based on the ionizing energy deposition within the SV. Although this is already a rather basic physical quantity, we must re-emphasize that the SEU actually will depend on the charge collected and not the charge deposited. To complicate the issue even further only the charge collected within a certain time window will be of importance. All these charge collection effects we do not consider. Ideally these effects could be the same for the heavy ions used in the tests and the fragments emitted from interactions and thus cancel out from our estimate. We are well aware that we probably are not that fortunate and some uncertainty from the charge collection efficiency for different ion species remains in our results. Moreover, we point out that the fixed parallelepiped shape of the SV is a crude approximation of reality and does not take into account effects such as funneling and enhanced charge collection due to bipolar effects and source-to-drain currents. These latter mechanisms have been shown to contribute significantly in modern devices [6,12].

Besides the limits listed above there are other potential sources of uncertainty in our simulation approach. Below we point out some inherent uncertainties related to the use of the event generators of FLUKA.

First, we have not yet directly verified that the underestimate of  $\alpha$ -production appears only at the low limit of the FLUKA energy range. Such underestimate led to the factor of 2 discrepancy in the SEU cross section at 20 MeV shown in Table 3. However, it is reasonable to assume that at higher energies, when more final states are accessible, errors due to wrong cross sections of individual channels cancel out.

We could also not verify the validity of the high-energy event generators of FLUKA, as all our comparison with proton data invoke only the pre-equilibrium model. Since only a rather small fraction of the particle spectrum at typical accelerators falls above the validity range of the pre-equilibrium model, the potential consequences of this uncertainty are rather limited.

A rather puzzling discrepancy is related to pion inelastic reactions. Experimental SEU data with pions indicates at about 200 MeV a significant enhancement of SEU rate compared to

protons of the same energy [15]. In our simulations we observe an enhancement which is only slightly more than the difference in inelastic cross sections. Contrary to a proton a pion can deposit all its rest mass in the nucleus and thus induce a very violent break-up reaction. It is, however, difficult to imagine that the number of recoil fragments could significantly increase. It is also experimentally established that the pion and proton bulk damages in silicon scale very well with the inelastic cross section [14], which to our mind should essentially exclude any significant increase in the number of fragments for pion reactions. The only possible explanation for an enhancement of pion induced upsets could be a break-up channel, which produces very energetic fragments. Also this seems surprising because quite a large cross section would be needed for this channel in order to explain a significant increase of SEU rate. However, there is some device-dependent spread also in the experimental data [13] and some devices seem to be rather consistent with our results while others are significantly higher. This issue should be clarified since a factor of 2 discrepancy for these low-energy pions would be almost fully reflected in our SEU predictions for the CMS inner tracker, where a large fraction of hadrons are just such pions.

Both the multi-GeV regime and the low-energy pions should be systematically tested with an IC which has been characterized in a heavy ion beam. Only then we could draw a firm conclusion how much off our simulation model is for these cases.

Finally we should point out that the hadron radiation environment which we will encounter at LHC is not exactly known and available simulations are assumed to be accurate within a factor of about 3. Thus, despite the uncertainties listed above, our method appears to have more than adequate accuracy for LHC applications.

## 10 Conclusion

Despite the approximations included in our model, the method we propose has shown good agreement with proton and neutron experimental data. This method allows to estimate the SEU rate which a given IC would experience in a hadron accelerator environment. Such an estimate can be easily computed using our available set of simulated energy deposition probabilities and the Weibull fits to heavy ion experimental data.

The application of this method to the radiation environment of CMS, one of the experiments at the future LHC collider, has shown that the SEU rate in a typical DRAM will be dominated in all regions of the experiment by hadrons with energy above 20 MeV. This result verifies that even in the experimental cavern, with a large flux of thermal neutrons, the  $^{10}\text{B}(n,\alpha)^7\text{Li}$  reaction is unlikely to play an important role. Furthermore neutrons below 20 MeV of energy seem to be responsible for about 10% of upsets only. This is a particularly welcome observation, because our method seems to require a rather good guess of the sensitive depth when studying low-energy neutron reactions, whereas this parameter is less important for the more energetic recoils emitted in high-energy scattering.

Our simulation results, obtained by applying first principles of the nuclear interactions of hadrons in silicon, combined with the finding that high-energy hadrons dominate the SEU rate at LHC, lead us to propose a simple method for generic testing of ICs intended for use in the LHC envi-



moment. Because the SEU cross section for high-energy hadrons is roughly energy-independent above some 30 MeV and drops rapidly below that energy, a suitable test would be to use a 60-200 MeV proton beam to irradiate the devices. This should provide a reasonable estimate of the SEU rate in most locations around the LHC. Only for inner trackers this might be too optimistic and a dedicated test in a pion beam of about 200 MeV would be closer to reality. The SEU cross section observed in a medium energy proton beam should be applied to the LHC hadron flux above 20 MeV. Or if a conservative estimate is desired this cut could be lowered down to a minimum of 2 MeV.

## 11 Acknowledgements

We wish to thank Dr. Eugene Normand from Boeing Information, Space & Defense Systems for fruitful discussions, always bringing new and interesting ideas. We are also grateful to Dr. G. Stefanini from CERN for his continuous interest and support of this work.

## References

- [1] G.C. Messenger, M.S. Ash, *Single Event Phenomena*, Chapman & Hall, 1997
- [2] A. Fassò, A. Ferrari, J. Ranft and P. Sala, Specialists' Meeting on Shielding Aspects of Accelerators, Targets and Irradiation Facilities. Arlington, Texas, April 28–29, 1994 NEA/OECD doc. p.287 (1995).
- [3] A. Fassò, A. Ferrari, J. Ranft and P. Sala, Proc IV Int. Conf. on Calorimetry in High Energy Physics, La Biodola, Sept. 20–25, 1993. Ed. A. Menzione and A. Scribano, World Scientific, p. 493 (1993).
- [4] R.J. Glauber and G. Matthiae, Nucl. Phys. B21 (1970) 135.
- [5] J.F. Ziegler, J.P. Biersack and U. Littmar, *The stopping and range of ions in solids*, Vol. 1, Pergamon Press (1985).
- [6] P.E. Dodd, *et al*, IEEE Trans. Nucl. Sci. Vol 43, No 6, (1996) 2797.
- [7] Heavy Ion & Proton SEE characterization Test Report, ESA/ESTEC Contract No. 11755/95/NL/NB-WO1/COO2, ESA Contract Report.
- [8] P.J.Griffin, *et al*, IEEE Trans. Nucl. Sci. Vol 44, No 6, (1997) 2079.
- [9] E. Normand, IEEE Trans. Nucl. Sci. Vol 45, No 6, (1998) 2904.
- [10] Ph. Calvel, *et al*, IEEE Trans. Nucl. Sci. Vol 43, No 6, (1996) 2827.
- [11] D. Thouvenot *et al.*, Neutron Single Event test results for various SRAM memories, in the 1997 NSREC Workshop Records.
- [12] C. Detcheverry, *et al*, IEEE Trans. Nucl. Sci. Vol.44, No 6, (1997) 2266
- [13] C.J.Gelderloos, *et al*, IEEE Trans. Nucl. Sci. Vol 44, No 6, (1997) 2237.
- [14] M. Huhtinen and P.A. Aarnio, Nucl. Instr. and Meth. A335 (1993) 580.  
P.A. Aarnio *et al*, Nucl. Instr. and Meth. A360 (1995) 521.